REPORT DOCUMENTATION PAGE

1. REPORT DATE *(DD-MM-YYYY)* 07-04-2009	2. REPORT TYPE Journal Article	3. DATES COVERED *(From - To)*

4. TITLE AND SUBTITLE

Identification of Helicon Plasma via Radial Magnetic Field Profiles (Preprint)

5a. CONTRACT NUMBER

5b. GRANT NUMBER

5c. PROGRAM ELEMENT NUMBER

6. AUTHOR(S)
Michael P. Reilly & George H. Miley (University of Illinois); William Lewis (ERC)

5d. PROJECT NUMBER

5e. TASK NUMBER

5f. WORK UNIT NUMBER
33SP0708

7. PERFORMING ORGANIZATION NAME(S) AND ADDRESS(ES)

Air Force Research Laboratory (AFMC)
AFRL/RZSS
1 Ara Road
Edwards AFB CA 93524-7013

8. PERFORMING ORGANIZATION REPORT NUMBER

AFRL-RZ-ED-JA-2009-145

9. SPONSORING / MONITORING AGENCY NAME(S) AND ADDRESS(ES)

Air Force Research Laboratory (AFMC)

AFRL/RZS
5 Pollux Drive
Edwards AFB CA 93524-7048

10. SPONSOR/MONITOR'S ACRONYM(S)

11. SPONSOR/MONITOR'S NUMBER(S)
AFRL-RZ-ED-JA-2009-145

12. DISTRIBUTION / AVAILABILITY STATEMENT

Approved for public release; distribution unlimited (PA #09163).

13. SUPPLEMENTARY NOTES
For publication in IEEE Transactions on Plasma Science.

14. ABSTRACT

The propagation of Helicon waves in 5 cm cylindrical plasma has been identified by radial Bz magnetic field profiles. These profiles are correlated with radial plasma density profiles which show a transition from a broad uniform density distribution during inductive plasma to centrally peaked profile during helicon wave propagation. Additionally, the matching network circuit parameters have been analyzed to show a sharp drop in reflected power when the discharge supports helicon waves. At times, the results of the matching network analysis for identification of helicon waves can be ambiguous. Likewise, identification of helicon waves through 'density jumps' or visual inspection can be misinterpreted or non-exact. The most accurate method of identifying helicon wave propagation is shown to be through measurement of radial magnetic field profiles.

15. SUBJECT TERMS

16. SECURITY CLASSIFICATION OF:			17. LIMITATION OF ABSTRACT	18. NUMBER OF PAGES	19a. NAME OF RESPONSIBLE PERSON Dr. Brian E. Beal
a. REPORT **Unclassified**	b. ABSTRACT **Unclassified**	c. THIS PAGE **Unclassified**	SAR	20	19b. TELEPHONE NUMBER *(include area code)* N/A

Identification of Helicon Plasma via Radial Magnetic Field Profiles
(Preprint)

Michael P Reilly and George H Miley

Department of Nuclear, Plasma, and Radiological Engineering and

University of Illinois @ Urbana-Champaign

William Lewis

Consultant for ERC INC.

The propagation of Helicon waves in 5 cm cylindrical plasma has been identified by radial B_z magnetic field profiles. These profiles are correlated with radial plasma density profiles which show a transition from a broad uniform density distribution during inductive plasma to centrally peaked profile during helicon wave propagation. Additionally, the matching network circuit parameters have been analyzed to show a sharp drop in reflected power when the discharge supports helicon waves. At times, the results of the matching network analysis for identification of helicon waves can be ambiguous. Likewise, identification of helicon waves through 'density jumps' or visual inspection can be misinterpreted or non-exact. The most accurate method of identifying helicon wave propagation is shown to be through measurement of radial magnetic field profiles.

Introduction

The use of radiofrequency discharges to generate helicon waves has long been studied for the application to materials processing [1-3]. More recently, this discharge has been suggested for use in plasma propulsion [4-8]. The primary attraction of this discharge for various applications comes from the reported high ionization efficiency [9]; nearly full ionization for modest input power (few hundred Watts). Additionally, the plasma density n_p is high $\sim 10^{13}$ cm^{-3} with a relatively low electron temperature $T_e \sim$ 3-4 eV for $\sim$ 1 kW input power [9-12].

Initially, identification of helicon wave propagation was based upon the magnetic field profile measurement with B-dot probes [10] and compared to the analytic treatment to the B field solutions in a cylindrical discharge subject to a uniform plasma density distribution [13]. For a given frequency, tube radius, and gas, the transmitted power to the discharge and the static

magnetic field B_0 could be varied (typically increased) until they very nearly satisfied the dispersion relation. At that point, the internal measured magnetic field profiles would nearly resemble the calculated profiles and the conclusion was that the dielectric could support the propagation of helicon waves. However, due to experimental difficulty or for other reasons, different methods of determining helicon wave propagation have been utilized. One such way has been through observation of 'density jumps' to identify the transition from capacitive or inductive plasma to helicon wave plasma. An additional method has been that of 'seeing' a bright blue or white 'core' in the center of the discharge. However, both these identifying traits can potentially be explained in terms of parasitic circuit losses [14] or neutral gas depletion in the center [15], respectively. Although both traits (density jump and visual identification of a core) can be characteristics of a helicon discharge, they are not necessarily mutually exclusive with the internal magnetic field profile to that of helicon wave propagation.

This article will examine the radial magnetic field profiles for the B_z component. Measurements are made from pressures of 0.5 mTorr – 10 mTorr on a 5 cm diameter quartz tube with an m=+1 antenna driven at 13.56 MHz. Magnetic fields of 300, 600, & 900 Gauss are tested at input power levels from 100-500 Watts. The onset of helicon wave propagation in each instance is examined via the B_z component.

Radial density profiles for the case of helicon waves at 10 mTorr and 900 Gauss are correlated with the B_z profiles for different power levels. Destruction of the helicon wave at the transitional power level is easily seen both through the B_z measurements and the density profile. For comparison with theory, a uniform density profile is used even though experimentally measured profiles exist. Use of the density profiles in predicting the shape of the radial magnetic field profiles has a negligible effect on the results; this will be discussed in further detail.

Additionally, the forward-to-reflected power ratio was analyzed and cross-referenced with these profiles. The results will clearly show that for some cases, identification of helicon waves by density jumps or circuit analysis is possible though ambiguous at certain operating conditions. The most effective and accurate way to identify helicon plasma is through measurement of the internal radial magnetic field profiles.

Theory

The derivation of an expression for the B-field due to the helicon plasma current has been thoroughly treated though the most comprehensive and cohesive analysis is given in Refs [11, 13, 16, 17]. It would be prudent to show that the analysis of helicon waves begins with a derivation for the dispersion relation based off of Maxwell's equations

$$\nabla \bullet B = 0 \tag{0.1}$$

$$\nabla \times E = i\omega B \tag{0.2}$$

$$\nabla \times B = \mu_0 (j - i\omega\varepsilon_0 E) \tag{0.3}$$

For plasma driven at ω_{rf} where $\omega_{ci} < \omega_{rf} < \omega_{ce}$ (driving frequency between ion and electron cyclotron frequencies); the frequency is high such that the ions are assumed to not move and low so that electron inertia is neglected. Therefore the plasma current is given by

$$\vec{j} = -en_0(r)\frac{\vec{E} \times \vec{B_0}}{B_0^2} \tag{0.4}$$

Perturbations of the form $\exp\left[i(m\theta + kz - \omega t)\right]$ are assumed and Maxwell's equations (for an arbitrary radial plasma density profile) can be reduced to the second order differential[18]

$$B_z'' + f(r)B_z' + g(r)B_z = 0 \tag{0.5}$$

where

$$f(r) = \frac{1}{r} - \frac{2\alpha\alpha'}{\beta} \tag{0.6}$$

$$g(r) = \frac{\beta}{\gamma} - \frac{m^2}{r^2} - \frac{m}{k}\frac{\alpha'}{\gamma r}\left(1 + \frac{2k^2\gamma^2}{\beta}\right) \tag{0.7}$$

$$\beta = \alpha^2 - k^2\gamma^2 \tag{0.8}$$

$$\alpha(r) = \frac{\omega}{k}\frac{e\mu_0 n_0(r)}{B_0} \tag{0.9}$$

$$\gamma = 1 - \left(\frac{k_0}{k}\right)^2 \tag{0.10}$$

$$k_0 = \frac{\omega}{c} \tag{0.11}$$

and k is assumed based off the antenna length. Equation (1.5) can be solved numerically based on a chosen radial density profile. Alternatively, for an assumed uniform density profile (no radial gradient) → $\alpha' = 0$, and if we neglect the displacement current so $k_0 = 0$ → $\gamma = 1$, then the solution to equation (1.5) can be solved analytically in terms of Bessel functions [9, 11, 13, 16]. Those results are shown in Figure 1.
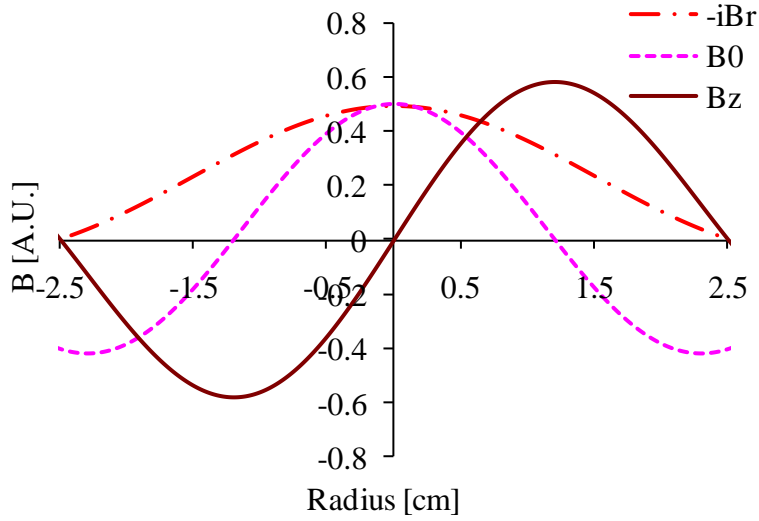
Figure 1. B-field solutions for a 2.5 cm radius helicon plasma with uniform radial density profile.

For a non-uniform density profile, the results are given in Ref [18] for density profiles of the form

$$\frac{n}{n_0} = \left[1 - \left(\frac{r}{a} \right)^s \right]^t \tag{0.12}$$

where 's' and 't' determine the degree of the density gradient. Once a profile is assumed or measured, the radial B-field can be determined. However, the important information to take away from this analysis is that as the density gradient increases from a broad profile to one that is steeper and more centrally peaked, the resulting form of the B_z profile shifts. This is illustrated in Figure 2.
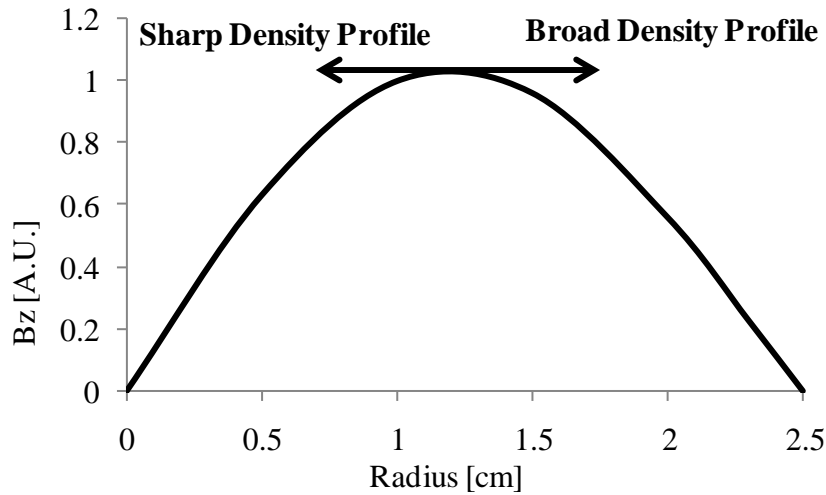
Figure 2. B$_z$ profile with density gradient dependence.

This is the component of interest that was measured in this work; the radial B_z field.

Experiment

This work was performed at the Air Force Research Laboratory's helicon testing facility. All tests were conducted on a 5 cm diameter quartz tube using Argon gas. Pressures from 0.5-10 mTorr were performed for 100 – 500 Watts input power at 300, 600, and 900 Gauss static B-field. Pressure was monitored with a MKS 629D Baratron capacitance manometer. An ENI A1000 linear power amplifier was used with a Bird 4421 power sensor and a Manitou Systems auto-match network. The antenna was a ½ turn helical m = +1 antenna; 20 cm in length and driven at 13.56 MHz. Argon gas was flowed in the direction of the magnetic field into a ½ meter diameter, 1 meter long stainless steel diffusion chamber. The entire schematic is shown in Figure 3.
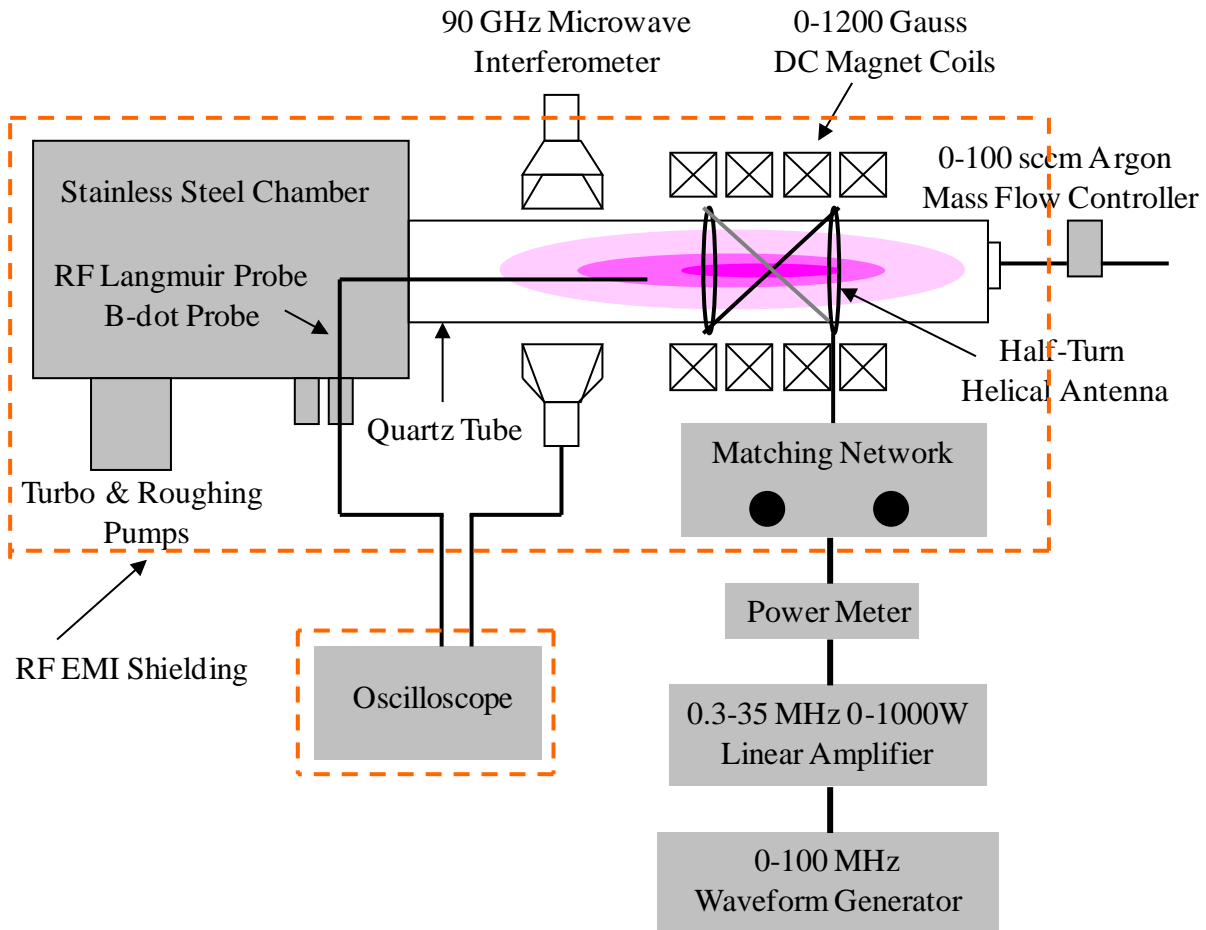
Figure 3. Schematic of AFRL Helicon Testing Facility.

Diagnostics

In order to thoroughly and accurately determine when the onset of helicon waves occurs, four different measurements were made. The first of these consisted of quantifying the applied static magnetic field by a Gauss meter. Following this, an examination of the forward and reflected power was conducted. Additionally, radial profiles of plasma density by a RF compensated Langmuir probe were performed as were measurements of the radial B_z profiles. All probe measurements were recorded on an oscilloscope housed inside a faraday cage built from solid copper sheets.

Static Magnetic Field

The propagation of helicon waves in plasma naturally requires the use of a static magnetic field. Toward this end, four electromagnetic coils were utilized that geometrically measured 45 cm in total length and provided a uniform magnetic field over approximately 30 cm. This DC field

was measured with an F.W. Bell Gauss meter (Model 7030). The determination of the static field for varying input currents is shown in Figure 4.
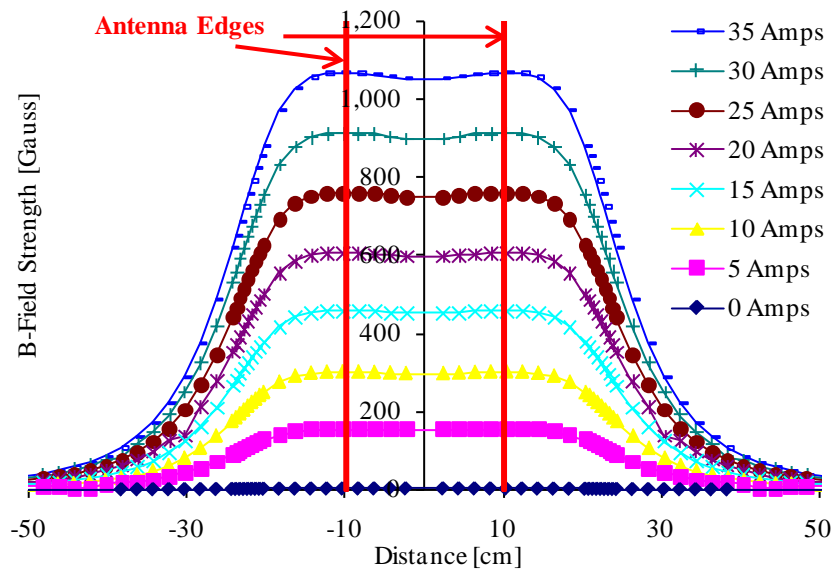
Figure 4. Axial Static Magnetic Field.

B-dot Probes

The magnetic induction probes used in this experiment consisted of two surface mount inductors spatially orientated 180 degrees with respect to each other and connected through a center tapped transformer in order to cancel any capacitive plasma effects. The probes were coated in a high temperature ceramic paste and housed in a 3 mm OD quartz tube that was vacuum sealed to protect the probe and ensure the plasma was free from contaminates. Careful attention was paid to cable and transmission line effects such that the probe was self-resonant at a frequency much higher that 13.56 MHz; frequency of interest. Complete characterization of the probes used in this work can be found in Ref. [19].

Often times in work with radio frequency plasma discharge, there exists the potential for probes to pickup 'noise' or spurious signal contributions from harmonics of the driving frequency. In the case of plasma driven at 13.56 MHz, harmonics of this fundamental can be found at 27.12 MHz, 40.68 MHz, 54.24 MHz, etc. These are contributions to the primary signal that are not filtered out by proper probe characterization and not necessarily due to plasma oscillations. To illustrate this point, we consider a raw magnetic probe signal obtained from plasma driven at 500 Watts with a 900 Gauss applied static magnetic field Figure 5. Additionally, we consider the Fast-Fourier Transform (FFT) of the raw signal in order to view contributions due to harmonics (Figure 6).
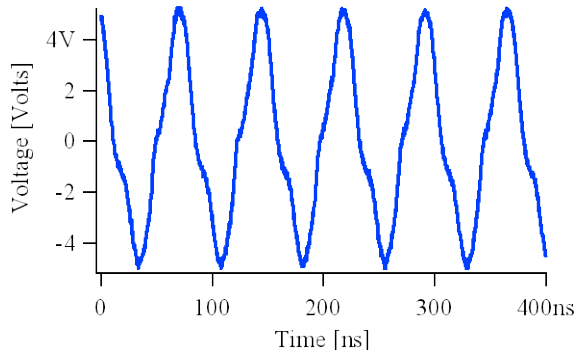
Figure 5. Raw Magnetic Probe Signal.
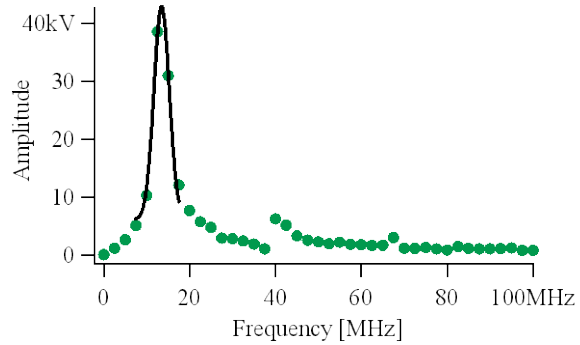
Figure 6. FFT of Raw Probe Signal.

Immediately obvious from Figure 5 is that the signal obtained is not a pure sinusoid. It has slight distortions due to frequency harmonic contributions. Similarly, Figure 6 shows clear contributions at the 3rd and 5th harmonics; 40.68 MHz and 67.80 MHz respectively. In order to accurately report what the fundamental (13.56 MHz) contribution is, a Gaussian fit was applied to the FFT in the vicinity of the fundamental and then the peak value used to calculate the amplitude; taken over the total number of data points; N=5000 in these tests. In this case, what appears to be a greater than 4 Volt amplitude signal from the raw data is actually a 3.43 Volt amplitude signal when the FFT is analyzed; or about 22.5% signal measurement error due to frequency harmonics.

As a more demonstrative example of frequency harmonic contribution, we consider a second raw data trace obtained in plasma shown in Figure 7. The signal appears much more distorted due to harmonic contributions and when we look at the FFT (Figure 8) of the raw data, we find contributions due to the 2nd, 3rd, 4th, 5th, 6th, and 7th harmonics. Again, fitting a Gaussian to the fundamental, we can calculate the signal amplitude to be 0.42 Volts where as upon inspection; the amplitude may be reported as ~0.70 Volts; (0.90+0.40)/2; or about a 67% signal measurement error.
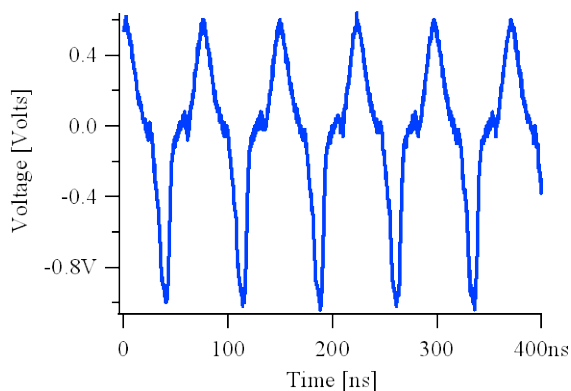
Figure 7. Raw Voltage Data Trace.
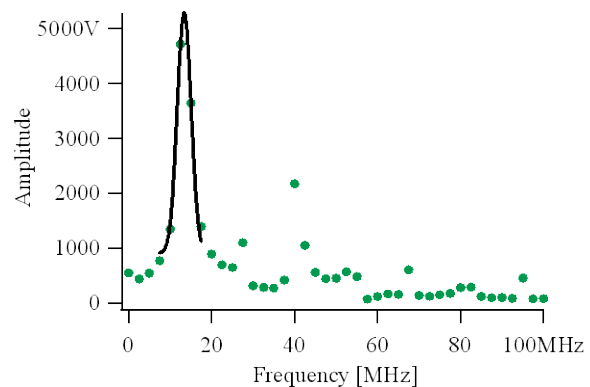
Figure 8. FFT of Raw Voltage Data Trace.

Obviously, in order to properly interpret results obtained from magnetic probes in plasma, it is necessary to remove any spurious contributions due to frequency harmonics. The most accurate method to accomplishing this is by recording the raw signal, performing a FFT, and taking the

peak of a Gaussian fit to the area of interest. Although, this can often be more time consuming than utilizing an RC integrating circuit before data acquisition in order to directly record the presumed magnetic field amplitude, it is the more accurate approach and allows the user to see harmonic contributions to the signal that will introduce error.

Langmuir Probe

In this work, a RF compensated Langmuir probe was constructed in-house with four notch filters; two at the fundamental and two at the second harmonic. Additionally, a 1 nF capacitor was placed between the measuring probe and compensation electrode Figure 9.
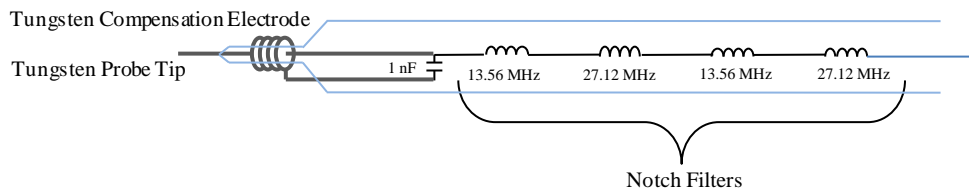
Figure 9. Schematic of Langmuir Probe Notch Filters and Compensation Circuitry.

The compensation electrode in conjunction with the notch filters provides a large choke impedance for the AC voltage component with respect to the plasma sheath impedance [20, 21]. For a typical inductive plasma this requires that the compensation electrode be on the order of a few nF's while the choke impedance be $\gg$ 1 kΩ [21-23]. This will limit the amount of AC current across the sheath that can distort the swept I-V curve as well as allowing the probe tip to be driven at voltage and follow plasma oscillations. The frequency response of the four notch filters in series is shown in Figure 10.
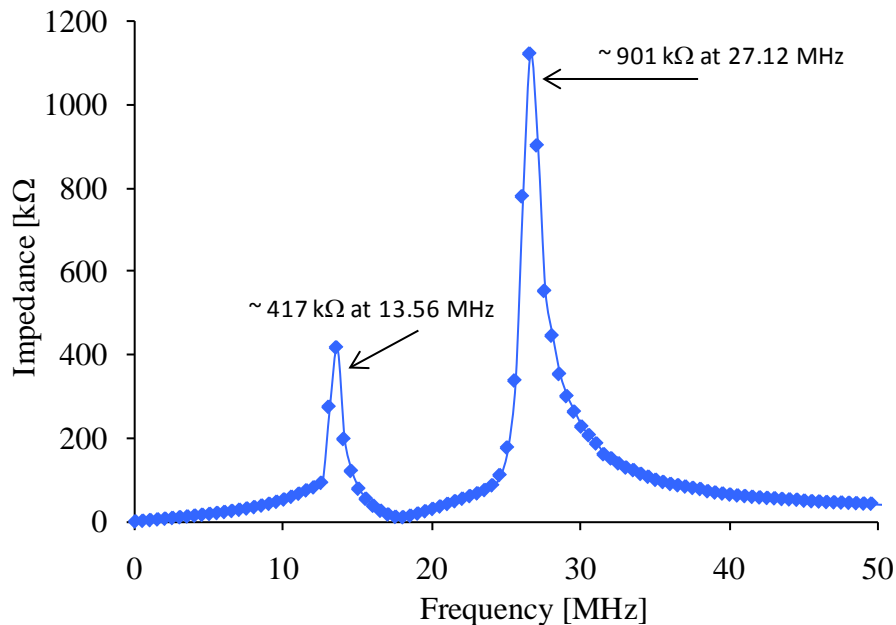
Figure 10. Impedance Curve for Four Series Notch Filters.

The filters are high frequency inductors from Vishay Dale where the series inductance and

parallel parasitic capacitance between the number of successive turns results in the resonance curve. Because each inductor is slightly different in the values of series inductance and parallel capacitance, the resonant frequency for each individual inductor will vary. Additionally, the manufacturer's listed self resonant frequency is not always exact due to non-testing of every single inductor. However, for our purpose, this was very important and consequently, hundreds of inductors impedance curves were analyzed. To do this quickly, efficiently, and accurately, frequency sweeps were performed with the Agilent 4294A Precision Impedance Analyzer. Sweeps can be made over a specified interval from 40 Hz – 110 MHz with up to 801 individual data points in < 1 s. This made it possibly to rapidly test many different inductors to determine which would yield the highest impedance at the fundamental and second harmonic frequencies.

Finally, the probe tip was swept from ± 100 Volts over 200 ms and the DC component of the current was measured across a 1 kΩ resistor. The measuring circuitry consisted of a Kepco Bi-polar voltage power supply, while the current was measured with a Tektronix P5205 100 MHz high voltage differential probe to minimize any common mode signal. The probe tip and compensation electrode were made from 0.009" diameter [0.02286 cm] tungsten wire. The probe tip was 4.0 mm in length while the compensation electrode was wound approximately 20 times on a 0.025" OD [0.0635 cm] alumina tube spanning 6.0 mm. This yielded an effective probe surface area of 2.91 mm^2 and a compensation electrode surface area of 18.87 mm^2; such that the compensation electrode's surface area was approximately 6.5 times as large as the probe's surface area.

An example of two raw I-V traces along with accompanying cubic spline fits are shown in Figure 11 and Figure 12.
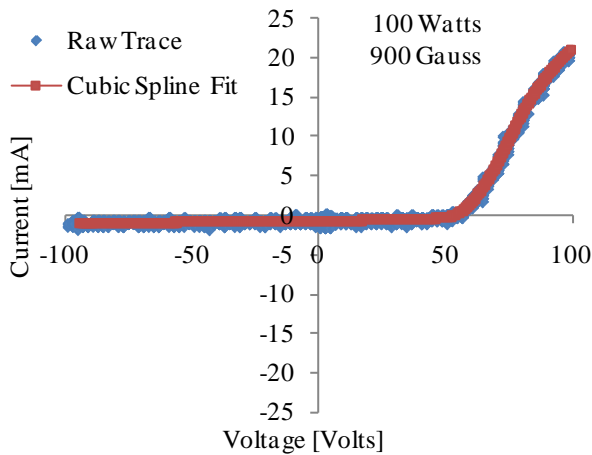
Figure 11. Langmuir Probe I-V trace

47 sccm; 10 mTorr; 100 Watt; 900 Gauss; 5 cm OD.
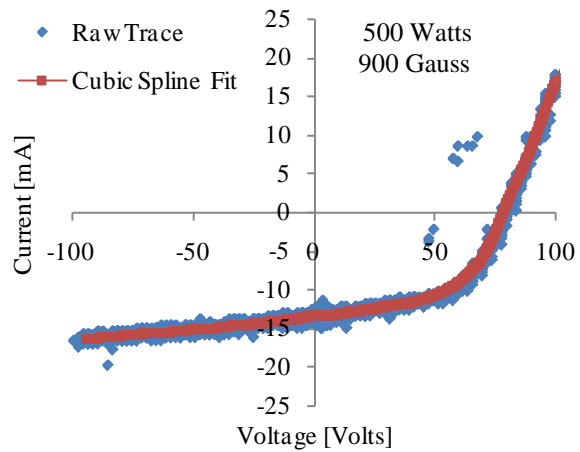
Figure 12. Langmuir Probe I-V trace

47 sccm; 10 mTorr; 500 Watt; 900 Gauss; 5 cm

For the purposes of this paper, only the plasma ion density will be reported as this has previously been a tool for determining the onset of helicon mode in plasma. In all the probe traces analyzed in this paper, Langmuir's orbital-motion-limited (OML) theory was utilized and the plasma density was determined through Dr. Francis Chen's OML analysis program according to

$$I_i \approx A_p ne \frac{\sqrt{2}}{\pi}\left(\frac{|eV_p|}{M}\right)^{1/2}$$

(0.13)

Results and Discussion

Results are provided for the forward and reflected power measurements, the radial plasma density profiles, and the radial magnetic field profiles for the axial component B_z at a variety of conditions. The control case for the following measurements will be a total input power of 500 Watts with a 900 Gauss applied static magnetic field operating at 47 sccm (~ 10 mTorr) Argon gas in a 5 cm OD quartz tube. However, a variety of input power levels and magnetic field strengths will be examined and discussed.

Forward / Reflected Power Measurements

A Bird 4421 RF power sensor was used to monitor the forward and reflected power from the RF generator to the auto-match network and antenna. The matching network configuration is shown below in Figure 13.
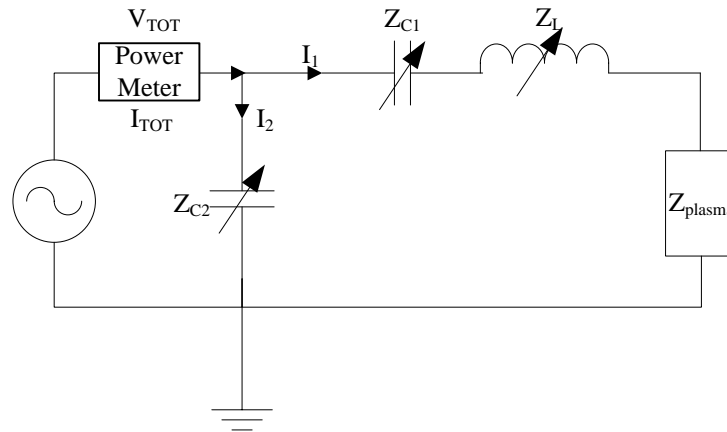
Figure 13. Schematic of Matching Network

For the case of a 5 cm diameter cylindrical, m=+1 plasma discharge, the forward and reflected power spectrum is shown in Figure 14 for various magnetic field strengths. During each condition, the reflected power begins as a minimum and then slowly increases as the input power is raised until some point where there is a 'sharp' decline in the reflected power. At this point, the power is said to couple more efficiently to the plasma and could be used as a method to identify the onset of helicon wave propagation. Also, Figure 14 shows that as the magnetic field is increased, the decline in reflected power occurs at a lower input power level. This is equivalent to analyzing the dispersion relation for helicon wave propagation [9, 11, 16, 17] that at a fixed frequency and magnetic field, the relation is satisfied once the density reaches a certain

value. And since density is proportional to input power [11], once the forward power level reaches this critical value for a given magnetic field, helicon waves can propagate.
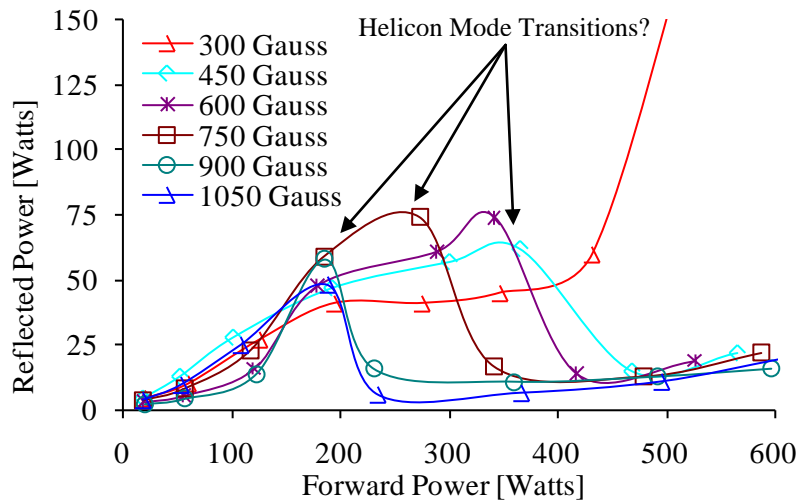
Figure 14. Forward vs. Reflected Power at 47 sccm; 10 mTorr fill pressure.

However, evidenced by these results is ambiguity in accurately knowing when the dispersion relation is satisfied. Since power loss can come in many forms, i.e, transmission line loss, radiated loss, antenna coupling efficiency, etc, utilizing the power spectrum as a method to identifying helicon wave propagation can be vague and inaccurate.

Density profiles

Another method that has been utilized to identify helicon waves has been by looking at the plasma density and specifically looking for when a density 'jump' occurs. This would be a sharp increase in density from an inductive discharge to helicon discharge. For the case of 900 Gauss static magnetic field on the same cylindrical tube, radial density profiles were analyzed for various input powers; Figure 15.
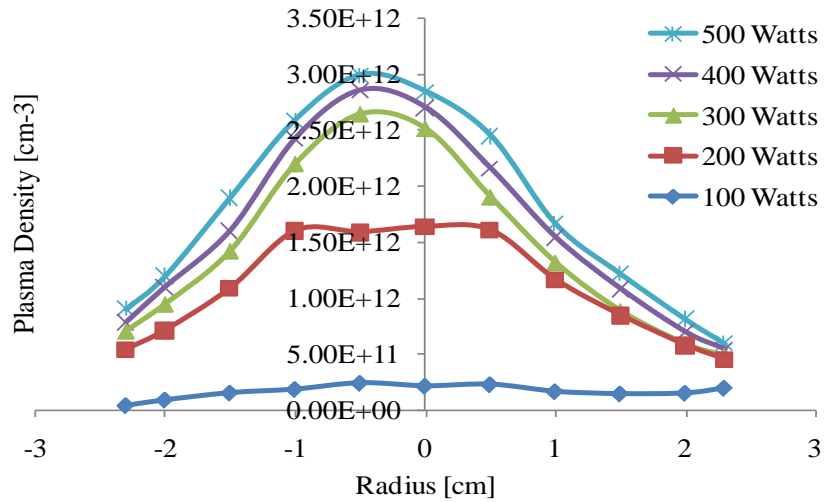
Figure 15. Radial plasma density profiles at 900 Gauss for various input power levels on a 5 cm diameter quartz tube at 13.56 MHz.

What can be inferred from these results coupled with the power spectrum analysis is that helicon wave plasma exhibits a radial parabolic profile whereas the inductive (lower power) discharge maintains a relatively flat density profile. As can be seen for the 200 Watt case, the 'small' Langmuir probe destroys the helicon wave from about -1 cm to 1 cm as the probe is swept radially through the discharge. However, at higher powers, the density is large enough to overcome the presence of the probe in order to maintain helicon wave propagation around the probe.

The peak density appears to be shifted slightly left of center (~ 0.5 cm) according to Figure 15; however, this can be attributed to several different factors. First, the alignment of the probe in the center of the quartz tube has some associated error as this was not given significant importance. Similarly, the centering of the quartz tube itself within the center of the magnets may not have been perfectly aligned. In order to ensure that the 'peak' did not shift or oscillate, radial profiles at different downstream locations from the antenna were taken and showed to consistently be shifted to the left of center.
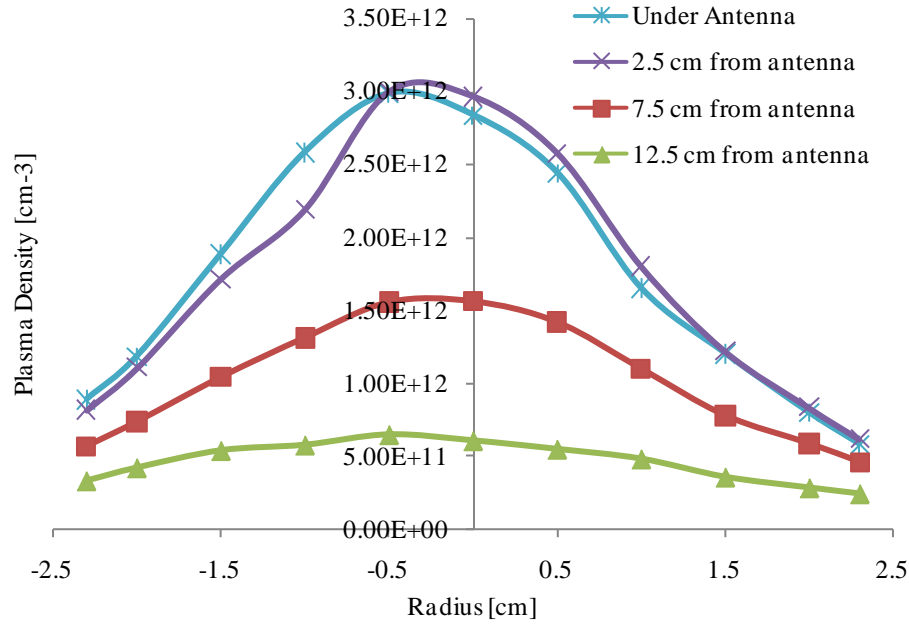
Figure 16. Downstream radial density profiles at 500 Watt, 900 Gauss.

Recently, the density jumps exhibited in Figure 15 have been shown to be manifestations of the matching network configuration (L-, T-, Π-), its component values (capacitances and inductances), as well as transmission lines [14]. Consequently, in both the case of analyzing the power spectrum and utilizing plasma density measurements, both methods can be unreliable and inaccurate at showing the propagation of helicon waves. Additionally, when starting the analysis of helicon waves, the only derived measurement is that for the internal magnetic fields. Therefore, it would seem natural that the sole method of accurately identifying helicon waves be done through measurement of the wave magnetic fields.

B_z profiles

Toward this end, the previously described B-dot probe was used to take radial scans underneath the antenna. It is necessary to perform scans here because the nature of the propagating helicon wave will not necessarily preserve its radial structure as it moves downstream of the antenna. This is the result of the calculated analytical solution assuming an infinitely long static magnetic field with uniform energy deposition, i.e., the source geometry has a finite antenna length and specific magnetic field structure (Figure 4). The radial scans for 47 sccm Argon (~10 mTorr) subject to the various input powers and peak applied fields are shown in Figure 17.
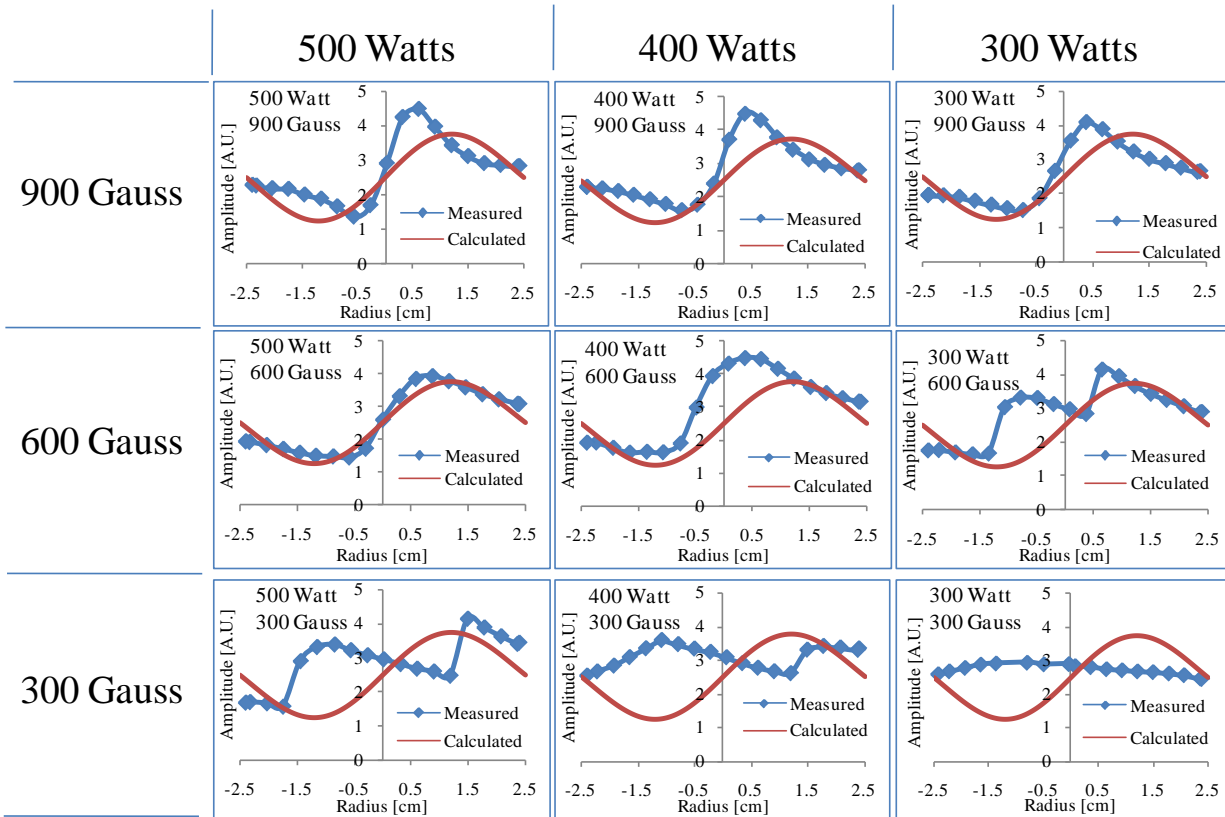
Figure 17. Internal plasma magnetic field profiles for 10 mTorr; 47 sccm; Argon gas in a 5 cm diameter quartz m=+1 tube with various input power and peak applied magnetic fields.

The calculated profiles, that the measured ones are compared against, are for an assumed uniform radial density profile. As discussed previously, a more parabolic density profile will lead to a shift in the peak of the B_z profiles toward the center. We show that this is consistent with the radial density scans for the 900 Gauss case as shown in Figure 15.

Additionally, for the lower field cases (600 Gauss), the measured profiles more closely agree with the analytic solution suggesting a more uniform radial density profile at these operating conditions. In the lower power and field cases shown in Figure 17 (300 Watt; 600 Gauss / 500 Watt; 300 Gauss / 400 Watt; 300 Gauss) the results show two discontinuities as the probe is scanned across the cross section of the discharge. These discontinuities are the result of the probes intrusion and destruction of the helicon wave. When the probe is against both walls, the bulk density is high enough that the dispersion relation is satisfied with the applied magnetic field. However, as the probe enters the center of the plasma discharge, the applied input power is not great enough that the density can overcome the presence of the probe. These results are also consistent with the radial density scans shown for the 200 Watt case in Figure 15 which indicates that the profile begins to have a parabolic shape, but then becomes flat as the probes presence destroys the helicon wave resulting in a flat density profile.

When analyzing the singular case of 900 Gauss for 300, 400, & 500 Watt input power levels (Figure 18), we find that the intensity of the internal field does not greatly increase with an increase in power level. Additionally, from Figure 15, we show that the density profiles and peak values don't necessarily vary greatly either. It should also be pointed out that for the radial B_z profiles shown Figure 18 that this is not a sinusoidal wave profile that goes from –a to +a (where 'a' is the radius). At first glance, Figure 18 seems to indicate that this is a wave with some fixed 'offset'. However, the values taken at each location are the resulting amplitudes of the FFT from the time varying magnetic field signal. So, there is no 'offset' here, but rather a wave amplitude value at each point taken on the cross section.
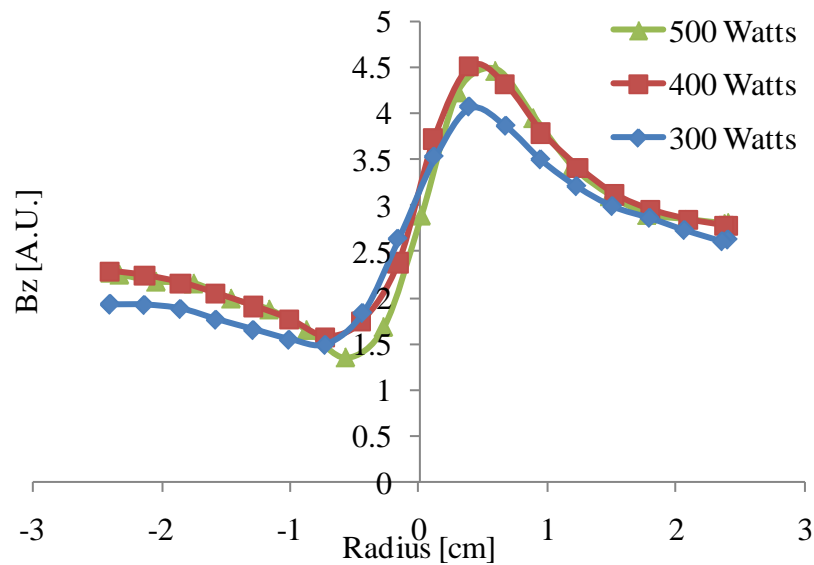
Figure 18. Radial Bz profiles for 47 sccm, 900 Gauss peak magnetic field at different input power levels.

In a separate analysis, this becomes important because the wave amplitude value increases and decreases as a full 3-D scan of the helicon wave is performed. Since this is a right-handed propagating wave, this result should be expected, but at the same time, this emphasizes the importance of performing the radial B_z scan underneath the end of the antenna; or at some integer value of the 'helicon wavelength'. Radial scans at different axial locations may not necessarily yield the same profile, i.e, at ½ λ of the helicon wave; the radial profile will be 'flipped' to that shown in Figure 19.
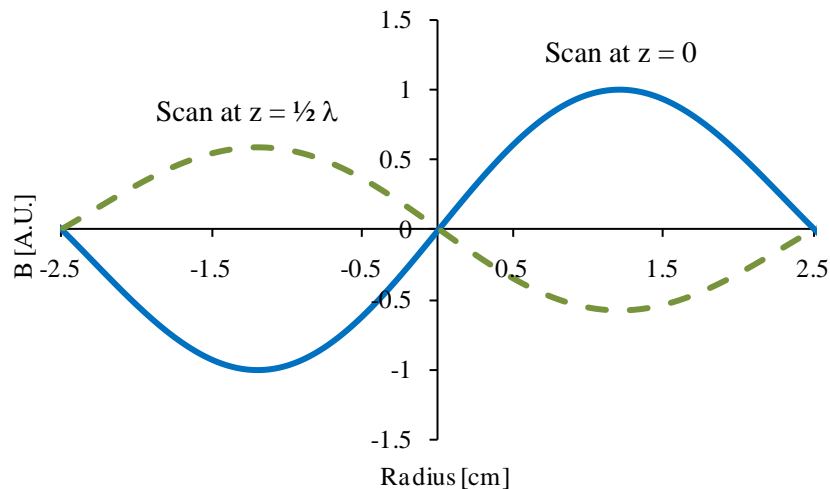
Figure 19. Expected radial B_z scan at axial locations indicating the importance of comparing analytic B_z profile with that measured under antenna region.

Radial scans for the B_z profiles were also done at pressures of 0.5, 2, 4, 6, & 8 mTorr and applied input powers up to 500 Watts and static magnetic fields of 900 Gauss. These results are not given here due to the large number of profiles that would be displayed; however the results are consistent with what has been shown thus far. They indicate that as the pressure decreases (for the same applied input power), the bulk density should likewise be expected to decrease. Additionally, this makes it more 'difficult' to satisfy the conditions for helicon waves. The result is that for a lower pressure and density, a higher magnetic field is required to propagate the wave; for a fixed frequency.

Conclusions

We have shown that the most accurate method toward identification of helicon waves is done through measurement of the analytic B_z profiles. This should be evident from the fact that analytical treatment directly leads to expressions for these profiles based on a given radial density profile (although typically assumed uniform). This is precisely the reason why the onset of helicon waves should not be identified through measurement of plasma density; it is one of the inputs for the analysis of helicon waves not one of the consequences of them. Similarly, ambiguity has been shown in the use of forward and reflected power measurements (or circuit analysis) as well as the use in some previous reports of 'pink', 'purple', and 'blue' mode for visual identification. While it is acknowledged that most of the identifiers used are traits inherent to helicon plasma, they are not exclusive to them alone and consequently, the radial B_z profiles should be used to correctly identify this type of discharge. Additionally we have shown that since high frequency measurements with magnetic field probes is often not easily implemented due to the nature of high frequency plasma, care in the calibration and construction

of diagnostics must be taken as well as in the post processing of data where one form of error can be manifest by not correctly accounting for harmonic distortion.

References

1.   Boswell, R.W. and D. Henry, *Pulsed high rate plasma etching with variable Si/SiO$_2$ selectivity and variable Si etch profiles.* Applied Physics Letters, 1985. **47**(10): p. 3.
2.   Perry, A.J., D. Vender, and R.W. Boswell, *The application of the helicon source to plasma processing.* Journal of Vacuum Science and Technology: B, 1991. **9**(2): p. 8.
3.   Goto, H.H., H.D. Lowe, and T. Ohmi, *Dual excitation reactive ion etcher for low energy plasma processing.* Journal of Vacuum Science & Technology A (Vacuum, Surfaces, and Films), 1992. **10**(5): p. 3048-54.
4.   Winglee, R., et al. *Mini-magnetospheric plasma propulsion (M2P2): High speed propulsion sailing the solar wind.* in *SPACE TECHNOLOGY AND APPLICATIONS INTERNATIONAL FORUM - 2000.* 2000. Albuquerque, New Mexico (USA): AIP.
5.   Arefiev, A.V., *Theoretical Studies of the VASIMR Plasma Propulsion Concept.* 2002, Texas at Austin. p. 120.
6.   Charles, C. and R.W. Boswell, *Laboratory evidence of a supersonics ion beam generated by a current-free "helicon" double layer.* Physics of Plasmas, 2004. **11**(4): p. 9.
7.   Squire, J.P., et al., *High power light gas helicon plasma source for VASIMR.* Thin Solid Films, 2006. **506-507**: p. 579-82.
8.   Walker, R., et al. *Experimental studies of helicon double layers for future high power plasma propulsion.* 2006. Sacramento, CA, United States: American Institute of Aeronautics and Astronautics Inc., Reston, VA 20191-4344, United States.
9.   Boswell, R.W., *Very Efficient Plasma Generation by Whistler Waves Near the Lower Hybrid Frequency.* Plasma Physics and Controlled Fusion, 1984. **26**(10): p. 16.
10.   Lehane, J.A. and P.C. Thonemann, *An experimental study of helicon wave propagation in a gaseous plasma.* Proceedings of the Physical Society 1965. **85**.
11.   Chen, F.F., *Plasma Ionization by Helicon Waves.* Plasma Physics and Controlled Fusion, 1991. **33**(4): p. 26.
12.   Chen, F.F., *Experiments on helicon plasma sources.* Journal of Vacuum Science and Technology: A, 1992. **10**(4): p. 13.
13.   Klozenberg, J.P., B. McNamara, and P.C. Thonemann, *The dispersion and attenuation of helicon waves in a uniform cylidrical plasma.* Journal Of Fluid Mechanics, 1965. **21**: p. 545-563.
14.   Chen, F.F. and H. Torreblanca, *Density jump in helicon discharges.* Plasma Sources Science and Technology, 2007. **16**(3): p. 593-596.
15.   Gilland, J.H., *Neutral pumping in a helicon discharge.* Plasma Sources Science and Technology, 1998. **7**: p. 416-422.
16.   Boswell, R.W., *A study of Waves in Gaseous Plasma*, in *School of Physical Sciences.* 1970, The Flinders University of South Australia.
17.   Chen, F.F., *Physics of helicon discharges.* Physics of Plasmas, 1996. **3**(5): p. 11.
18.   Chen, F.F., M.J. Hsieh, and M. Light, *Helicon waves in non-uniform plasma.* Plasma Sources Science and Technology, 1994. **3**: p. 9.
19.   Reillly, M.P., W. Lewis, and G.H. Miley, *Magnetic Field Probes for use in Radio Frequency Plasma.* Review of Scientific Instruments, Expected 2009.
20.   Godyak, V.A. and R.B. Piejak, *Probe measurements of the space potential in a radio frequency discharge.* Journal of Applied Physics, 1990. **68**(7): p. 6.

21.   Sudit, I.D. and F.F. Chen, *RF compensated probes for high-density discharges.* Plasma Sources Science and Technology, 1994. **3**: p. 7.

22.   Godyak, V.A. and R.B. Piejak, *Abnormally low electron energy and heating-mode transition in a low-pressure argon RF discharge at 13.56 MHz.* Physical Review Letters, 1990. **65**(8): p. 996-9.

23.   Godyak, V.A., R.B. Piejak, and B.M. Alexandrovich, *Measurements of electron energy distribution in low-pressure RF discharges.* Plasma Sources Science and Technology, 1992. **1**: p. 36-58.